Distinct regional patterns in noradrenergic innervation of the rat prefrontal cortex

Juan-Carlos Cerpa, Alain Marchand, Etienne Coutureau

Distinct regional patterns in noradrenergic innervation of the rat prefrontal cortex

Juan-Carlos Cerpa[1,2], Alain R. Marchand[1,2]*, Etienne Coutureau[1,2]*

[1]CNRS, Institut de Neurosciences Cognitives et Intégratives d'Aquitaine, UMR 5287, 33076 Bordeaux, France;

[2]Universite de Bordeaux, 33076 Bordeaux, France.

*A.M. and E.C. contributed equally to this work.

Address for correspondance: Etienne Coutureau

Institut de Neurosciences Cognitives et Intégratives d'Aquitaine (INCIA)

UMR 5287 CNRS/Université de Bordeaux

Université de Bordeaux-Site Carreire,

146 rue Léo Saignat, BP 31

33076 Bordeaux cedex

France

Phone: +33 (0)5 57 57 15 48

Fax: +33 (0)5 56 90 02 78

E-mail: etienne.coutureau@cnrs.fr

Running title: NA innervation of the Rat PFC

Abstract

The anatomy and functions of the rodent prefrontal cortex (PFC) have been extensively studied. It is now clear that the PFC is at the core of various executive functions and that these functions depend on monoaminergic neuromodulation. The PFC receives extensive projections from monoaminergic nuclei and, in particular, from the locus cœruleus (LC) which is the major source of noradrenaline (NA) in the cortex. Projections of this nucleus have long been considered to act diffusely and uniformly throughout the entire brain. However, recent studies have revealed a separate innervation of prefrontal sub-regions by non-collateralizing LC neurons, suggesting a specific modulation of their functions. Following this idea, we aimed at describing more precisely the pattern of noradrenergic innervation into different orbital (OFC) and medial (mPFC) sub-regions of the PFC. We focused on the lateral (LO), ventral (VO) and medial (MO) portions of the OFC, and on areas 32d (A32d), 32v (A32v) and 25 (A25) in the mPFC. Using Dopamine-β-Hydroxylase as a specific noradrenergic marker, we performed an automatic quantification of noradrenergic fibers and varicosities in each of these sub-regions. The results indicate that noradrenergic innervation is heterogeneous in some prefrontal sub-regions along the rostro-caudal axis. Functional dissociations have been recently reported in prefrontal sub-regions along the rostro-caudal direction. Our findings add neuroanatomical support to this emergent idea.

Keywords:

Prefrontal cortex

Noradrenaline

Orbitofrontal cortex

Prelimbic cortex

Infralimbic cortex

Neuroanatomy

1. Introduction

Seminal research has produced valuable descriptions of the neuroanatomy and functions of the prefrontal cortex (PFC) of humans, non-human primates and rodents (Carmichael and Price, 1995, 1996; Goldman and Nauta, 1977; Ongur and Price, 2000). In the rat, the PFC can be divided into several areas that include the medial prefrontal cortex (mPFC) and the orbitofrontal cortices (OFC) (Fuster, 2015; Heidbreder and Groenewegen, 2003; Hoover and Vertes, 2011; Laubach *et al.*, 2018; Uylings *et al.*, 2003; Vertes, 2004). These regions are critical actors underlying executive functions, including memory, attention, decision-making and behavioral flexibility (Dalley *et al.*, 2004; Schoenbaum *et al.*, 2009; Uylings *et al.*, 2003). Furthermore, recent studies point to an even greater parcellation, which could depend on the architecture of afferent and efferent patterns of connection along the anteroposterior and mediolateral axes (Bradfield *et al.*, 2018; Izquierdo, 2017; Killcross and Coutureau, 2003; Panayi and Killcross, 2018).

The function of these PFC regions (Arnsten, 2000; Arnsten *et al.*, 1999; Bouret and Sara, 2004; Lammel *et al.*, 2011; Ren *et al.*, 2018; Tronel *et al.*, 2004; Usher *et al.*, 1999) is known to be greatly influenced by the neuromodulatory actions of dopamine, serotonin (5-HT) and noradrenaline (NA) (Beier *et al.*, 2015; Chandler *et al.*, 2013; Hoover and Vertes, 2007; Linley *et al.*, 2013; Murphy and Deutch, 2018). In particular, the PFC receives extensive projections from the locus coeruleus (LC) in the brainstem, which is the major source of NA in the cortex (Berridge and Waterhouse, 2003; but see Robertson *et al.*, 2013). Earlier studies have shown an important and widespread noradrenergic innervation of various cortical regions (Foote *et al.*, 1983; Fuxe *et al.*, 1968; Levitt and Moore, 1978; Lewis and Morrison, 1989; Morrison *et al.*, 1978), which was thought to result from significant branching from single NA axons. This idea has been recently contradicted by data showing that individual LC neurons independently innervate different prefrontal regions (Chandler *et al.*, 2014; Chandler *et al.*, 2013; Kebschull *et al.*, 2016; Uematsu *et al.*, 2017). However, the

precise organization of NA innervation into the different orbitofrontal and medial regions along their rostro-caudal axis is not well documented.

With this in mind, we performed a detailed analysis of the different prefrontal sub-regions using an automatic quantification method. Our results show that noradrenergic innervation distributes homogeneously into most OFC and mPFC sub-regions. However, we found a specific pattern of innervation along the rostro-caudal axis of the most ventral part of the mPFC and the OFC suggesting a particular route for afferent noradrenergic fibers innervating different prefrontal subregions.

2. Material & Methods

2.1. Animals and housing conditions

A total of 11 male Long-Evans rats, aged 2-3 months, were obtained from Centre d'Elevage Janvier (France). Rats were housed in pairs. Environmental enrichment was provided by orange-tinted polycarbonate tubing elements. The facility was maintained at 21 ± 1 °C with lights on from 08:00 to 20:00. The animals of this study previously served as a control group in unpublished study and had received an intra-cerebral injection of an inactive form of saporin. As in our previous papers (see e.g.Parkes *et al.*, 2018), injection were made using a thin glass pipette which minimizes damage to the surrounding areas. As a result and as shown previously, there was no gliosis or any damage at the site of injection that could affect the observed pattern of results. The experiments were conducted in agreement with French (council directive 2013-118, February 1, 2013) and international (directive 2010-63, September 22, 2010, European Community) legislations and received approval # 5012053-A from the local Ethics Committee.

2.2. Immunohistochemistry

At the age of 5-6 months, rats were killed with an overdose of pentobarbital monosodic and perfused transcardially with 60 ml of saline followed by 260 ml of 4% paraformaldehyde (PFA) in 0.2 M phosphate buffer (PB). Brains were removed and postfixed in the same PFA

solution overnight and then transferred to a 0.1M PB solution. Subsequently, 40 µm coronal sections were cut using a VT1200S Vibratome (Leica Microsystems). Every fourth section was collected to form a series and immunoreactivity was performed for Dopamine-β-Hydroxylase (DBH). Free-floating sections were first rinsed in phosphate buffer saline containing 0.3% Triton X-100 (PBST; 4x5 min) and then incubated in a blocking solution (PBST 3% containing 3% goat serum) for 1h. Sections were then incubated with mouse monoclonal anti-DBH antibody (1/10 000 in blocking solution, Millipore Bioscience Research Reagents) for 48h at 4 °C on a shaker. After further rinses in PBS 0.1 M (4x5 min), sections were placed for 2h in a bath containing biotinylated goat anti-mouse secondary antibody (1/1000 in PBST 0.3%, Jackson ImmunoResearch) for 90 min at room temperature. Following rinses in PBS 0.1 M (4x5 min), they were then incubated with avidin-biotin-peroxydase complex (1/200 in PBS 0.1 M, ThermoFisher Scientific) for 90 min at room temperature. The final staining was made with a diaminobenzidine (DAB, Sigma-Aldrich) and hydrogene peroxide solution. Sections were rinsed with Tris buffer 0.05 M and then PB 0.05 M. They were collected on gelatin-coated slides, dehydrated with xylene, mounted and coverslipped using Eukitt mounting medium.

2.3. Quantification of fiber density

Sections were scanned using a Nanozoomer slide scanner (Hamamatsu Photonics) with 20x lens and analyzed with the NDP.view 2 freeware (Hamamatsu Photonics). Digital microphotographs of regions of interest (ROI) in each hemisphere were examined under 20x. virtual lens. Each ROI was outlined according to Paxinos and Watson (2014). In the OFC, we examined both VO and LO at coordinates (AP+ from Bregma) +4.4, +3.7 and +3.0 and MO at coordinates +5.6, +5.1 and +4.4. In the mPFC, we examined both A32d (corresponding to dorsal portion of prelimbic cortex with very limited extension into cingulate cortex, according to Paxinos and Watson (2007)) and A32v (corresponding to ventral portion of prelimbic cortex) at coordinates +4.4, +3.7, +3.0. And at coordinates +3.0 and +2.5 for A25 (infralimbic

cortex). For each section, we analyzed square windows (300 x 300 µm, 1320 x 1320 pixels) corresponding to the different structures (Figure 1).

Quantification of DBH-positive fibers was performed using an automated method developed in the laboratory using ImageJ software (**Supplemental material S1**). To estimate the density of fibers in an area of interest, a digitized version of the microphotograph was converted to black and white by combining blue, red and green channels with weights 1, -0.25 and -0.25, then subjected to a median filter (radius 3 pixels) in order to improve signal-to-noise ratio. It was then smoothed with a Gaussian filter (radius 8) and subtracted from the previous picture to isolate high spatial frequencies. Large stains were further eliminated by detecting them in a copy of the image. The picture was then subjected to a fixed threshold (grey level 11) to extract stained elements, and the relative volume occupied by fibers was estimated by the proportion of detected pixels in the ROI. As a control for poor focus, the same images were analyzed again while allowing lower spatial frequencies (Gaussian filter radius 20). The ratio between the proportions of pixels detected by the two methods was used as a criterion to eliminate blurry images (representing 1.2 % of total images).

Automated quantification of varicosities (**Supplemental material S2**) was performed on the blue channel of each image by smoothing the image with two different Gaussian filters (radius 5 and 2.5) and subtracting the results (Difference of Gaussians) in order to select blobs of the appropriate size. The result was then subjected to a fixed threshold (grey level 18). Highly stained spots of slightly more than 1 µm in diameter were detected, corresponding to enlargements (varicosities) on the DBH fibers (Figure 2). Like for fibers, our measure was the proportion of detected pixels in the ROI, since it appeared to be a more robust measure than the number of detected spots.

2.4. Data analyses

Measurements of the density of fibers and varicosities were analyzed via ANOVAs. The ratio of varicosities to fibers was also analyzed. Measurements from both hemispheres of the same animal were averaged at each anatomical level. Data from different antero-posterior coordinates were treated as repeated measures. ANOVAs were followed, when required, by Fisher's PLSD *post hoc* tests. Datasets for all regions of interest passed Shapiro-Wilk test for normality, with the exception of ratio data for VO where the results were confirmed using Kruskal-Wallis non parametric analysis. Analyses were performed using Statview software (SAS institute). The α value for rejection of the null hypothesis for both ANOVAs and *post hoc* tests was fixed at 0.05. Data are presented as mean ± SEM.

3. Results

Figure 1 shows the location of the various regions of interest on sections of the PFC at different coordinates (AP+ from Bregma). We used these coordinates to examine the distribution of DBH fibers along the rostro-caudal axis for each structure of interest.

Our automated method also provided the distribution of varicosities for each region of interest.

Add FIG1 (2 columns)

Figure 2 shows a representative case illustrating both treatments applied to original images (Figure 2A). The method identifies DBH fibers (Figure 2B), and highly stained spots (Figure 2C) corresponding to varicosities (Agster *et al.*, 2013).

Add FIG2 (2 columns)

3.1. Pattern of NA innervation in the OFC

We first examined the distribution of noradrenergic fibers into the MO, LO and VO along the rostro-caudal axis. Figure 3A shows the density of DBH-immunoreactive fibers for each region at different levels anterior to Bregma (AP+4.4; AP+3.7; AP+3.0 for LO & VO and AP+5.6; AP+5.1; AP+4.4 for MO). Representative images are shown in Figure 3C. Analyses

highlighted the homogeneity of distribution of DBH fibers along the antero-posterior axis for both MO ($F_{(2,14)}$ = 0.49; ns) and LO ($F_{(2,20)}$ = 0.91; ns) but not for VO ($F_{(2,20)}$ = 25.561; p<0.0001). Post hoc analyses revealed significant differences between AP+4.4 and both AP+3.7 (p<0.0001) and AP+3.0 (p<0.0001) and between AP+3.7 and AP+3.0 (p=0.04) for VO, indicating an increasing gradient of DBH fibers from the anterior part to the most posterior part. Comparison between VO and LO at the same three coordinates shows an effect of Region ($F_{(1,10)}$ = 22.158; p = 0.0008), an effect of Coordinates ($F_{(2,20)}$ = 11.089; p = 0.0006) and an interaction between Region and Coordinates ($F_{(2,20)}$ = 36.855; p < 0.0001), indicating a different distribution of DBH fibers into these two regions.

Add FIG3 (2 columns)

In addition, we also performed these analyses for highly stained spots corresponding to varicosities. Results are shown in Figure 3B. ANOVAs for same regions revealed an effect of Coordinates for LO ($F_{(2,20)}$ = 3.602; p = 0.04). Post hoc analysis indicated a significant difference between AP+4.4 and both AP+3.7 (p=0.04) and AP+3.0 (p=0.02). No effect of Coordinates was found for MO ($F_{(2,14)}$ = 0.605; ns). Surprisingly, the statistical analysis showed no significant effect of Coordinates for VO ($F_{(2,20)}$ = 2.247; ns), despite an observable increase of DBH spots density at AP+3.7 and AP+3.0. However, ANOVA analyses on VO and LO revealed a decrease in the ratio varicosities/fibers along their antero-posterior axis (Figure 3C, $F_{(2,20)}$ = 5.949; p = 0.0094) with no effect of Region ($F_{(1,10)}$ = 4.542; ns). These results suggest the presence of a higher number of fibers of passage, presenting fewer varicosities, at the most caudal portion of VO.

3.2. Pattern of NA innervation in the mPFC

Figure 4A shows the density of DBH-immunoreactive fibers for three regions of the mPFC (A32d, A32v and A25) at different levels anterior to Bregma (AP+3.0; AP+2.5 for A25 and AP+4.4; AP+3.7; AP+3.0 for both A32d and A32v). Representative images are shown in Figure 3B. The ANOVA revealed an homogenous density of DBH-stained fibers along the

rostro-caudal axis of A32d ($F_{(2,18)}$ = 1.221; ns) and A32v ($F_{(2,18)}$ = 0.04; ns). Further analyses comparing both structures with Coordinates and Region as factors showed neither an effect of Region ($F_{(1,8)}$ = 0.686; ns) or Coordinates ($F_{(2,16)}$ = 0.413; ns) and no Region x Coordinates interaction ($F_{(2,16)}$ = 3.157; ns), indicating a stable and equivalent distribution of DBH-fibers along the rostro-caudal axis in each of these two regions. By contrast, an effect of Coordinates was found for A25 ($F_{(1,10)}$ = 9.959; p = 0.0102).

Add FIG4 (2 columns)

Complementary analyses (Figure 4B) showed homogeneity of varicosities along the rostro-caudal axis of A32d ($F_{(2,19)}$ = 0.946; ns) and A32v ($F_{(2,18)}$ = 1.158; ns) but not A25 ($F_{(1,10)}$ = 5.451; p = 0.04). Analysis of the ratio varicosities/DBH-fibers (Figure 4C) in A32d and A32v showed no effect of Coordinates ($F_{(2,16)}$ = 1.170; ns) or Region ($F_{(1,8)}$ = 2.649; ns). The ratio was also constant in A25 where we found no effect of Coordinates ($F_{(1,10)}$ = 1.172; ns).

4. Discussion

Using detection of DBH-immunoreactive fibers, the present study shows a distinctive pattern of NA innervation of the rat PFC. DBH fibers volume occupancy was relatively uniform when compared between prefrontal regions at the same level of the rostro-caudal axis. However, when examining each area along the rostro-caudal axis, we found a specific gradient of innervation for both VO and A25 (infralimbic cortex). Moreover, the ratio of varicosities to fibers decreased caudally in both VO and LO regions. These results have important implications for our understanding of the prefrontal areas which are detailed below.

4.1. Methodological considerations

While the intensity and specificity of DBH detection may vary according to each particular antibody, the anti-DBH antibody used in this study only marked regions classically reported to receive noradrenergic innervation, and the morphology of immunoreactive fibers and

varicosities was consistent with that of earlier reports (Agster *et al.*, 2013; Grzanna *et al.*, 1977; Lewis and Morrison, 1989; Morrison *et al.*, 1979).

In the present study, we deliberately used the regional boundaries defined in the latest Paxinos and Watson atlas (Paxinos and Watson, 2014). The choice of using new and not previous boundaries, which included prelimbic and infralimbic terms (Paxinos and Watson, 2007), is based on evidence for homologies among medial parts of the PFC, especially the anterior cingulate cortex (ACC), in rodents, humans, and monkeys (Vogt, 1993; Vogt *et al.*, 2013; Vogt and Paxinos, 2014). In order to obtain the best possible fit between each micrograph and the diagrams provided by the atlas, we used multiple anatomical landmarks thus allowing to pool data from several subjects while minimizing imprecision concerning the boundaries of the sub-regions. For each region of interest, we avoided both superficial and deep layers and restricted our analyses to a central portion where DBH staining was homogeneous, in order to compare the density of fibers along the rostro-caudal axis. The automated analysis employed here is much less labor intensive than the stereological method. Instead of focusing on the numerical density of varicosities (Agster *et al.*, 2013), our method can provide an estimate of both the relative volume occupied by fibers (Naneix *et al.*, 2012; Naneix *et al.*, 2013) and by varicosities, which potentially yield distinct information. Nevertheless, we cannot present our data as a strict quantification of noradrenergic innervation in prefrontal regions. Rather, we aimed to highlight the rostro-caudal distribution of noradrenergic inputs into different sub-regions of medial and orbital portions of the PFC.

4.2. Patterns of rostro-caudal distribution

Our data largely agree with previous research in both rodents and primates, which suggest that noradrenergic innervation of the cortex is largely diffuse and homogeneous (Schwarz *et al.*, 2015). The density of varicosities has been reported to be higher in prefrontal regions than in other cortical regions (Agster *et al.*, 2013), suggesting that noradrenergic modulation plays a specific role in the PFC (Aston-Jones and Cohen, 2005; Bouret and Sara, 2005). Many of the fibers in these regions run in the frontal plane for tens

or hundreds of micrometers and present many varicosities (Figures 2-4), which may indicate that they are involved in distributing NA locally (Papadopoulos and Parnavelas, 1991). When considering each area of the PFC globally, we found little overall differences in the amount of innervation from LC. However, the main finding of the present study is the observation of a subtle rostro-caudal gradient of NA innervation in both the orbitofrontal and medial frontal regions.

In the medial regions, NA innervation appears homogenous in the dorsal (A32) but not in the ventral portion (A25), where DBH fibers volume occupancy is higher at most caudal levels. Such a pattern is also found when the amount of varicosities is considered. The constant ratio between varicosities and fibers found in A25 strongly suggests that the rostro-caudal gradient in density is not due to fibers of passage. Rather, the noradrenergic innervation appears intrinsically more important in the posterior part of A25 than in the anterior part, so that NA action might markedly differ. Interestingly, an opposite gradient in dopaminergic innervation has been reported in the same region (Naneix *et al.*, 2013), which points to important functional differences in this region along the rostro-caudal axis.

In orbitofrontal regions, the NA innervation appears homogenous in the medial and lateral portions. However, our results demonstrate a distinctive pattern in the VO where DBH fibers volume occupancy is higher in the most caudal portion, as in A25. Interestingly however, the ratio between varicosities and fiber occupancy decreases as one moves caudally in both VO and LO. A low ratio of varicosities to fibers may be an indication of a larger proportion of fibers of passage.

Add FIG5 (2 columns)

The distinct pattern of NA innervation in VO and A25 might result from their specific location in relation to the trajectory of ascending noradrenergic neurons. Past research has suggested that different noradrenergic ascending pathways reach the cerebral cortex. Both the mPFC and the MO/VO are innervated by the medial pathway that runs through the septum and curves over the genu of the corpus callosum (Morrison *et al.*, 1981). A more lateral projection leaves the medial forebrain bundle and proceeds laterally to innervate

lateral cortical areas in longitudinal strips. It is therefore likely that an important number of fibers of passage cross orbital regions to reach more dorsal and lateral sub-regions. Thus, the increasing ratio of varicosities to fibers that we observe rostrally may be attributed to a reduction in the number of fibers of passage as they stop upon reaching their target.

In order to contrast the results obtained when looking at intermediate laminae, we performed the same analysis in more superficial layers of A32v and A25 as representative cases. Indeed, earlier studies reported a stronger innervation in superficial layers of medial cortices (Agster *et al.*, 2013; Audet *et al.*, 1988; Descarries *et al.*, 1977; Fuxe *et al.*, 1968). In both A32v and A25, we also observed a stronger innervation in superficial layers. Moreover our results yielded a pattern of fiber distribution similar to that obtained in intermediate layers, suggesting that the rostro-caudal distribution of noradrenergic afferents holds across layers.

4.3. Functional Implications

In the present study, we provide anatomical evidence for a dissociation in the distribution of fibers and varicosities. Varicosities are swellings with high DBH concentration in which NA could be stored and released via en passant synapses or allowing volume transmission without synaptic contact (Agnati *et al.*, 1995; Chiti and Teschemacher, 2007; Descarries and Mechawar, 2000; Miner *et al.*, 2003). Activity, and therefore function, of each sub-region could then be modulated by such a mechanism in specific ways in accordance with recent propositions (Agster *et al.*, 2013; Chandler and Waterhouse, 2012; Sadacca *et al.*, 2016).

There is a growing body of evidence that the prefrontal cortex is innervated by heterogeneous pools of LC neurons with largely non-overlapping efferent connectivity (Chandler *et al.*, 2013; Uematsu *et al.*, 2017). In parallel, current research has demonstrated a definite parcellation of the functions subserved by the different regions (Coutureau and Parkes, 2018) in both the mPFC (Coutureau *et al.*, 2012; Killcross and Coutureau, 2003) and the OFC (Bradfield *et al.*, 2015; Parkes *et al.*, 2018). Moreover, a recent study provided evidence for a functional dissociation between anterior and posterior regions of the MO (Bradfield *et al.*, 2018). While we did not observe corresponding anatomical differences in

MO, other prefrontal regions such as A25 clearly show a heterogeneous NA innervation along the rostro-caudal axis. The present results thus add to this field by providing anatomical evidence that NA transmission might be substantially different both within and between prefrontal regions.

ACKNOWLEDGEMENTS

The microscopy was completed at the Bordeaux Imaging Center, a service unit of CNRS-INSERM and Bordeaux University and member of the national infrastructure, France BioImaging. We thank Y. Salafranque for the care provided to the rats during experiments. The authors wish also to thank Drs Shauna Parkes and Mathieu Wolff for their useful comments on an earlier version of this manuscript.

FUNDING

This work was supported by the French National Research Agency (grant number ANR-14-CE13-0014 GOAL to E.C); and by the Fondation pour la Recherche Médicale (FRM grant number ECO20160736024 to J-C.C).

References

Agnati, L.F., Zoli, M., Stromberg, I., Fuxe, K., 1995. Intercellular communication in the brain: wiring versus volume transmission. Neuroscience 69, 711-726.

Agster, K.L., Mejias-Aponte, C.A., Clark, B.D., Waterhouse, B.D., 2013. Evidence for a regional specificity in the density and distribution of noradrenergic varicosities in rat cortex. J Comp Neurol 521, 2195-2207.

Arnsten, A.F., 2000. Through the looking glass: differential noradenergic modulation of prefrontal cortical function. Neural Plast 7, 133-146.

Arnsten, A.F., Mathew, R., Ubriani, R., Taylor, J.R., Li, B.M., 1999. Alpha-1 noradrenergic receptor stimulation impairs prefrontal cortical cognitive function. Biological Psychiatry 45, 26-31.

Aston-Jones, G., Cohen, J.D., 2005. An integrative theory of locus coeruleus-norepinephrine function: adaptive gain and optimal performance. Annu Rev Neurosci 28, 403-450.

Audet, M.A., Doucet, G., Oleskevich, S., Descarries, L., 1988. Quantified regional and laminar distribution of the noradrenaline innervation in the anterior half of the adult rat cerebral cortex. J Comp Neurol 274, 307-318.

Beier, K.T., Steinberg, E.E., DeLoach, K.E., Xie, S., Miyamichi, K., Schwarz, L., Gao, X.J., Kremer, E.J., Malenka, R.C., Luo, L., 2015. Circuit Architecture of VTA Dopamine Neurons Revealed by Systematic Input-Output Mapping. Cell 162, 622-634.

Berridge, C.W., Waterhouse, B.D., 2003. The locus coeruleus-noradrenergic system: modulation of behavioral state and state-dependent cognitive processes. Brain Res Brain Res Rev 42, 33-84.

Bouret, S., Sara, S.J., 2004. Reward expectation, orientation of attention and locus coeruleus-medial frontal cortex interplay during learning. 20, 791-802.

Bouret, S., Sara, S.J., 2005. Network reset: a simplified overarching theory of locus coeruleus noradrenaline function. Trends Neurosci 28, 574-582.

Bradfield, L.A., Dezfouli, A., van Holstein, M., Chieng, B., Balleine, B.W., 2015. Medial Orbitofrontal Cortex Mediates Outcome Retrieval in Partially Observable Task Situations. Neuron 88, 1268-1280.

Bradfield, L.A., Hart, G., Balleine, B.W., 2018. Inferring action-dependent outcome representations depends on anterior but not posterior medial orbitofrontal cortex. Neurobiology of Learning and Memory.

Carmichael, S.T., Price, J.L., 1995. Sensory and premotor connections of the orbital and medial prefrontal cortex of macaque monkeys. J Comp Neurol 363, 642-664.

Carmichael, S.T., Price, J.L., 1996. Connectional networks within the orbital and medial prefrontal cortex of macaque monkeys. J Comp Neurol 371, 179-207.

Chandler, D., Waterhouse, B.D., 2012. Evidence for broad versus segregated projections from cholinergic and noradrenergic nuclei to functionally and anatomically discrete subregions of prefrontal cortex. Front Behav Neurosci 6, 20.

Chandler, D.J., Gao, W.J., Waterhouse, B.D., 2014. Heterogeneous organization of the locus coeruleus projections to prefrontal and motor cortices. Proc Natl Acad Sci U S A 111, 6816-6821.

Chandler, D.J., Lamperski, C.S., Waterhouse, B.D., 2013. Identification and distribution of projections from monoaminergic and cholinergic nuclei to functionally differentiated subregions of prefrontal cortex. Brain Res 1522, 38-58.

Chiti, Z., Teschemacher, A.G., 2007. Exocytosis of norepinephrine at axon varicosities and neuronal cell bodies in the rat brain. FASEB J 21, 2540-2550.

Coutureau, E., Esclassan, F., Di Scala, G., Marchand, A.R., 2012. The role of the rat medial prefrontal cortex in adapting to changes in instrumental contingency. PLoS One 7, e33302.
Coutureau, E., Parkes, S.L., 2018. Cortical Determinants of Goal-Directed Behavior, In: Morris, R., Bornstein, A., Shenhav, A. (Eds.), Goal-Directed Decision Making. Academic Press, pp. 179-197.
Dalley, J.W., Cardinal, R.N., Robbins, T.W., 2004. Prefrontal executive and cognitive functions in rodents: neural and neurochemical substrates. Neuroscience and Biobehavioral Reviews 28, 771-784.
Descarries, L., Mechawar, N., 2000. Ultrastructural evidence for diffuse transmission by monoamine and acetylcholine neurons of the central nervous system. Prog Brain Res 125, 27-47.
Descarries, L., Watkins, K.C., Lapierre, Y., 1977. Noradrenergic axon terminals in the cerebral cortex of rat. III. Topometric ultrastructural analysis. Brain Res 133, 197-222.
Foote, S.L., Bloom, F.E., Aston-Jones, G., 1983. Nucleus locus ceruleus: new evidence of anatomical and physiological specificity. Physiol Rev 63, 844-914.
Fuster, J.M., 2015. Anatomy of the Prefrontal Cortex, In: Fuster, J.M. (Ed.), The Prefrontal Cortex (Fifth Edition). Academic Press, pp. 9-62.
Fuxe, K., Hamberger, B., Hokfelt, T., 1968. Distribution of noradrenaline nerve terminals in cortical areas of the rat. Brain Res 8, 125-131.
Goldman, P.S., Nauta, W.J., 1977. Columnar distribution of cortico-cortical fibers in the frontal association, limbic, and motor cortex of the developing rhesus monkey. Brain Res 122, 393-413.
Grzanna, R., Morrison, J.H., Coyle, J.T., Molliver, M.E., 1977. The immunohistochemical demonstration of noradrenergic neurons in the rat brain: The use of homologous antiserum to dopamine-beta-hydroxylase. Neurosci Lett 4, 127-134.
Heidbreder, C.A., Groenewegen, H.J., 2003. The medial prefrontal cortex in the rat: evidence for a dorso-ventral distinction based upon functional and anatomical characteristics. Neuroscience and Biobehavioral Reviews 27, 555-579.
Hoover, W.B., Vertes, R.P., 2007. Anatomical analysis of afferent projections to the medial prefrontal cortex in the rat. Brain Struct Funct 212, 149-179.
Hoover, W.B., Vertes, R.P., 2011. Projections of the medial orbital and ventral orbital cortex in the rat. J Comp Neurol 519, 3766-3801.
Izquierdo, A., 2017. Functional Heterogeneity within Rat Orbitofrontal Cortex in Reward Learning and Decision Making. J Neurosci 37, 10529-10540.
Kebschull, J.M., Garcia da Silva, P., Reid, A.P., Peikon, I.D., Albeanu, D.F., Zador, A.M., 2016. High-Throughput Mapping of Single-Neuron Projections by Sequencing of Barcoded RNA. Neuron 91, 975-987.
Killcross, S., Coutureau, E., 2003. Coordination of actions and habits in the medial prefrontal cortex of rats. Cerebral Cortex 13, 400-408.
Lammel, S., Ion, D.I., Roeper, J., Malenka, R.C., 2011. Projection-specific modulation of dopamine neuron synapses by aversive and rewarding stimuli. Neuron 70, 855-862.
Laubach, M., Amarante, L.M., Swanson, K., White, S.R., 2018. What, If Anything, Is Rodent Prefrontal Cortex? eNeuro 5.
Levitt, P., Moore, R.Y., 1978. Noradrenaline neuron innervation of the neocortex in the rat. Brain Res 139, 219-231.
Lewis, D.A., Morrison, J.H., 1989. Noradrenergic innervation of monkey prefrontal cortex: a dopamine-beta-hydroxylase immunohistochemical study. J Comp Neurol 282, 317-330.
Linley, S.B., Hoover, W.B., Vertes, R.P., 2013. Pattern of distribution of serotonergic fibers to the orbitomedial and insular cortex in the rat. J Chem Neuroanat 48-49, 29-45.
Miner, L.H., Schroeter, S., Blakely, R.D., Sesack, S.R., 2003. Ultrastructural localization of the norepinephrine transporter in superficial and deep layers of the rat prelimbic prefrontal cortex and its spatial relationship to probable dopamine terminals. J Comp Neurol 466, 478-494.
Morrison, J.H., Grzanna, R., Molliver, M.E., Coyle, J.T., 1978. The distribution and orientation of noradrenergic fibers in neocortex of the rat: an immunofluorescence study. J Comp Neurol 181, 17-39.

Morrison, J.H., Molliver, M.E., Grzanna, R., Coyle, J.T., 1979. Noradrenergic innervation patterns in three regions of medial cortex: an immunofluorescence characterization. Brain Res Bull 4, 849-857.
Morrison, J.H., Molliver, M.E., Grzanna, R., Coyle, J.T., 1981. The intra-cortical trajectory of the coeruleo-cortical projection in the rat: a tangentially organized cortical afferent. Neuroscience 6, 139-158.
Murphy, M.J.M., Deutch, A.Y., 2018. Organization of afferents to the orbitofrontal cortex in the rat. J Comp Neurol 526, 1498-1526.
Naneix, F., Marchand, A.R., Di Scala, G., Pape, J.R., Coutureau, E., 2012. Parallel maturation of goal-directed behavior and dopaminergic systems during adolescence. J Neurosci 32, 16223-16232.
Naneix, F., Marchand, A.R., Pichon, A., Pape, J.R., Coutureau, E., 2013. Adolescent stimulation of D2 receptors alters the maturation of dopamine-dependent goal-directed behavior. Neuropsychopharmacology 38, 1566-1574.
Ongur, D., Price, J.L., 2000. The organization of networks within the orbital and medial prefrontal cortex of rats, monkeys and humans. Cerebral Cortex 10, 206-219.
Panayi, M.C., Killcross, S., 2018. Functional heterogeneity within the rodent lateral orbitofrontal cortex dissociates outcome devaluation and reversal learning deficits. Elife 7.
Papadopoulos, G.C., Parnavelas, J.G., 1991. Monoamine systems in the cerebral cortex: evidence for anatomical specificity. Prog Neurobiol 36, 195-200.
Parkes, S.L., Ravassard, P.M., Cerpa, J.C., Wolff, M., Ferreira, G., Coutureau, E., 2018. Insular and Ventrolateral Orbitofrontal Cortices Differentially Contribute to Goal-Directed Behavior in Rodents. Cerebral Cortex 28, 2313-2325.
Paxinos, G., Watson, C., 2007. The Rat Brain in Stereotaxic Coordinates (Sixth Edition). Academic Press.
Paxinos, G., Watson, C., 2014. The Rat Brain in Stereotaxic Coordinates (Seventh edition). Academic Press.
Ren, J., Friedmann, D., Xiong, J., Liu, C.D., Ferguson, B.R., Weerakkody, T., DeLoach, K.E., Ran, C., Pun, A., Sun, Y., Weissbourd, B., Neve, R.L., Huguenard, J., Horowitz, M.A., Luo, L., 2018. Anatomically Defined and Functionally Distinct Dorsal Raphe Serotonin Sub-systems. Cell.
Robertson, S.D., Plummer, N.W., de Marchena, J., Jensen, P., 2013. Developmental origins of central norepinephrine neuron diversity. Nat Neurosci 16, 1016-1023.
Sadacca, B.F., Wikenheiser, A.M., Schoenbaum, G., 2016. Toward a theoretical role for tonic norepinephrine in the orbitofrontal cortex in facilitating flexible learning. Neuroscience.
Schoenbaum, G., Roesch, M.R., Stalnaker, T.A., Takahashi, Y.K., 2009. A new perspective on the role of the orbitofrontal cortex in adaptive behaviour. Nat Rev Neurosci 10, 885-892.
Schwarz, L.A., Miyamichi, K., Gao, X.J., Beier, K.T., Weissbourd, B., DeLoach, K.E., Ren, J., Ibanes, S., Malenka, R.C., Kremer, E.J., Luo, L., 2015. Viral-genetic tracing of the input-output organization of a central noradrenaline circuit. Nature 524, 88-92.
Tronel, S., Feenstra, M.G., Sara, S.J., 2004. Noradrenergic action in prefrontal cortex in the late stage of memory consolidation. Learn Mem 11, 453-458.
Uematsu, A., Tan, B.Z., Ycu, E.A., Cuevas, J.S., Koivumaa, J., Junyent, F., Kremer, E.J., Witten, I.B., Deisseroth, K., Johansen, J.P., 2017. Modular organization of the brainstem noradrenaline system coordinates opposing learning states. Nat Neurosci 20, 1602-1611.
Usher, M., Cohen, J.D., Servan-Schreiber, D., Rajkowski, J., Aston-Jones, G., 1999. The role of locus coeruleus in the regulation of cognitive performance. Science 283, 549-554.
Uylings, H.B., Groenewegen, H.J., Kolb, B., 2003. Do rats have a prefrontal cortex? Behav Brain Res 146, 3-17.
Vertes, R.P., 2004. Differential projections of the infralimbic and prelimbic cortex in the rat. Synapse 51, 32-58.
Vogt, B.A., 1993. Structural Organization of Cingulate Cortex: Areas, Neurons, and Somatodendritic Transmitter Receptors, In: Vogt, B.A., Gabriel, M. (Eds.), Neurobiology of Cingulate Cortex and Limbic Thalamus: A Comprehensive Handbook. Birkhäuser Boston, Boston, MA, pp. 19-70.

Vogt, B.A., Hof, P.R., Zilles, K., Vogt, L.J., Herold, C., Palomero-Gallagher, N., 2013. Cingulate area 32 homologies in mouse, rat, macaque and human: cytoarchitecture and receptor architecture. J Comp Neurol 521, 4189-4204.
Vogt, B.A., Paxinos, G., 2014. Cytoarchitecture of mouse and rat cingulate cortex with human homologies. Brain Struct Funct 219, 185-192.

Figure Captions

Figure 1. Delimitation of prefrontal sub-regions

Location of regions of interest on frontal sections at different coordinates (indicated by numbers above and under each microphotograph), anterior to Bregma. Coordinates are based on Paxinos and Watson (2014). Squares represent analyzed area. Scale bars = 1mm. (LO = lateral OFC; VO = ventral OFC; MO = medial OFC).

Figure 2. Example of fibers and varicosities extraction by automated treatments

Illustration of images obtained after both automated treatments applied to the original picture. First treatment allows extraction of fibers signal in white pixels. Second treatment permits extraction of highly stained spots corresponding to varicosities in white pixels. Scale bar = 50 µm.

Figure 3. Pattern of noradrenergic innervation in OFC sub-regions

(A) Quantification of DBH-stained fibers in MO (blue bars), LO (orange bars) and VO (green bars) at different antero-posterior coordinates taken from Bregma (Paxinos and Watson, 2014). (B) Similar quantification of varicosities in the same sub-regions and at the same coordinates. (C) Ratio between varicosities and DBH-stained fibers at each coordinate. (D) Representative microphotographs of DBH-stained fibers for each sub-region along the rostro-caudal axis. *p≤0.05; **p≤0.01; ***p≤0.001. Scale bar = 100 µm.

Figure 4. Pattern of noradrenergic innervation in mPFC sub-regions

(A) Quantification of DBH-stained fibers in A32d (orange bars), A32v (green bars) and A25 (blue bars) at different antero-posterior coordinates taken from Bregma (Paxinos and Watson, 2014). (B) Similar quantification of varicosities in the same sub-regions and at the same coordinates. (C) Ratio between varicosities and DBH-stained fibers at each coordinate (D) Representative microphotographs of DBH-stained fibers for each sub-region along the rostro-caudal axis. *p≤0.05. Scale bar = 100 µm.

Figure 5. Scheme of a prefrontal noradrenergic innervation

Schematic representation of possible trajectories of noradrenergic afferents originating in the locus cœruleus and crossing VO. Lateral coordinate is taken from Bregma (Paxinos and Watson, 2014). Increase in varicosities proportion at more anterior levels is due to decrease in number of fibers of passage. Dotted arrows represent noradrenergic prefrontal innervation not studied in this article.

Supplementary material

Supplemental material S1. Automated method for fibers extraction in ImageJ software

```
// save file name for results
name=getTitle();run("Rename...", "title=full");
run("Set Measurements...", "area mean redirect=None decimal=3");
// extract blue component in ROI
run("Split Channels");
// subtract part of red and green
selectWindow("full (red)");run("Multiply...", "value=0.25");
selectWindow("full (green)");run("Multiply...", "value=0.25");
imageCalculator("Subtract", "full (blue)","full (red)");
imageCalculator("Subtract", "full (blue)","full (green)");
selectWindow("full (green)");close();
selectWindow("full (red)");close();
// select ROI 300x300µm
makeRectangle(790, 144, 1320, 1320);
run("Duplicate...", " ");run("Rename...", "title=data");
selectWindow("full (blue)");close();
// detect stains
run("Duplicate...", " ");run("Rename...", "title=stains");
run("Gaussian Blur...", "sigma=4.5");
run("Subtract Background...", "rolling=50 light");
setThreshold(0.0000, 220.0000);setOption("BlackBackground", true);run("Convert to Mask");
// filter image (salt and pepper)
```

```
selectWindow("data");
run("Median...", "radius=3");
// remove low spatial frequencies
run("Duplicate...", " ");run("Rename...", "title=fond");
run("Gaussian Blur...", "sigma=8");
imageCalculator("Subtract create 32-bit", "fond", "data");run("Rename...", "title=res");
// threshold
setThreshold(11.0000, 255.0000);setOption("BlackBackground", true);run("Convert to Mask");
// remove stains
imageCalculator("Subtract", "res", "stains")
selectWindow("stains");close();
// filter again
selectWindow("res");
run("Median...", "radius=2");
// count proportion of white pixels and insert file name
run("Measure");setResult("Image", nResults-1, name);
selectWindow("data");close();
selectWindow("fond");close();
```

Supplemental material S2. Automated method for varicosities extraction in ImageJ software

```
// save file name for results
name=getTitle();run("Rename...", "title=full");
run("Set Measurements...", "area mean redirect=None decimal=3");
// extract blue component in ROI
run("Split Channels");
selectWindow("full (green)");close();
selectWindow("full (red)");close();
// select ROI 300x300µm
makeRectangle(790, 144, 1320, 1320);
run("Duplicate...", " ");run("Rename...", "title=data");
selectWindow("full (blue)");close();
```

```
// compute difference of Gaussian
run("Duplicate...", " ");run("Rename...", "title=sharp");
run("Duplicate...", " ");run("Rename...", "title=smooth");
run("Gaussian Blur...", "sigma=5");
selectWindow("sharp");
run("Gaussian Blur...", "sigma=2.5");
imageCalculator("Subtract create", "smooth","sharp");run("Rename...", "title=res");
selectWindow("smooth");close();
selectWindow("sharp");close();
selectWindow("data");close();
// Threshold
setThreshold(18.0000, 255.0000);setOption("BlackBackground", false);run("Convert to Mask");
// count proportion of white pixels and insert file name
run("Measure");setResult("Image", nResults-1, name);
```

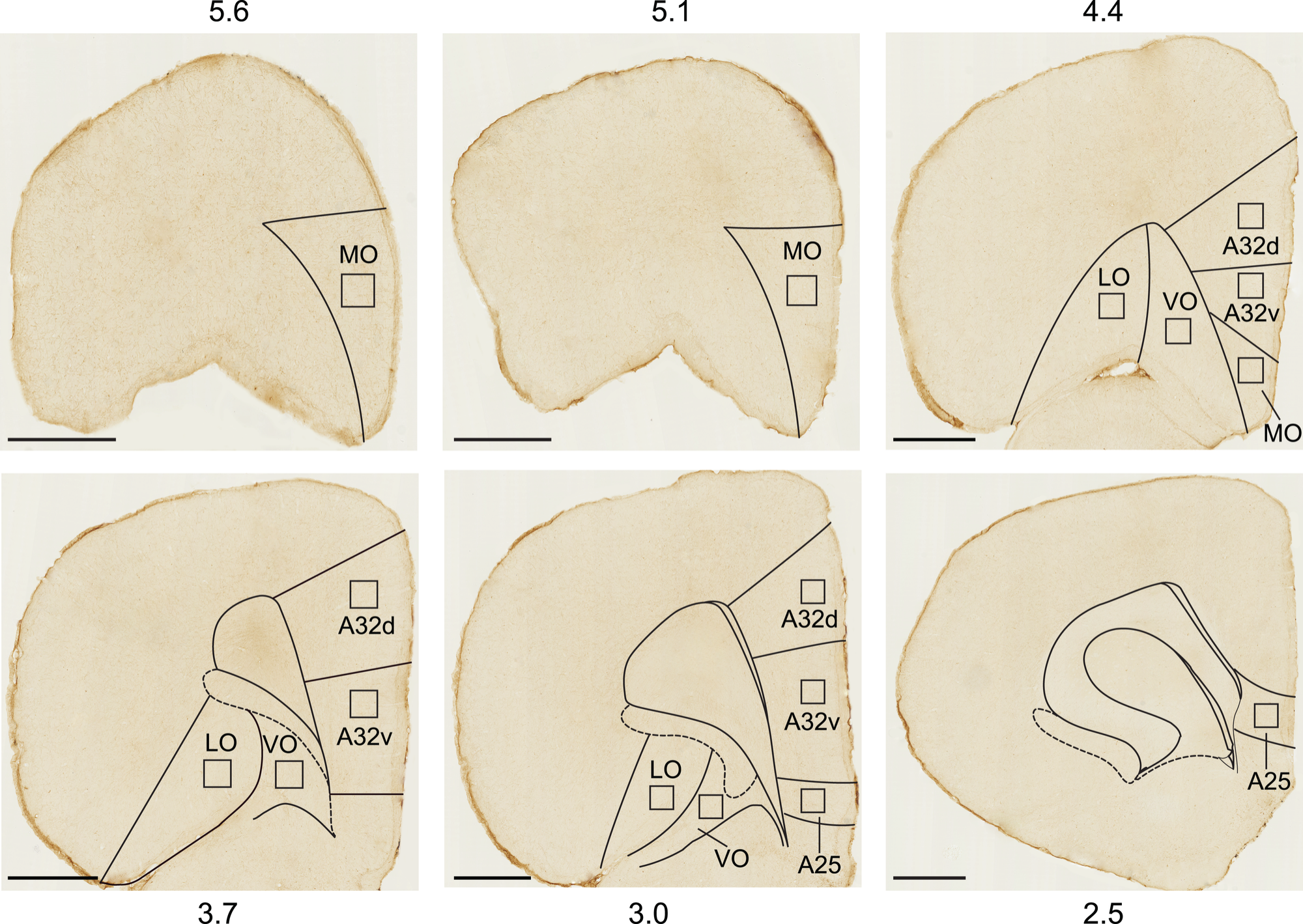
5.6
MO
5.1
MO
4.4
A32d
LO
VO
A32v
MO
A32d
LO
VO
A32v
3.7
A32d
LO
A32v
VO
A25
3.0
A25
2.5

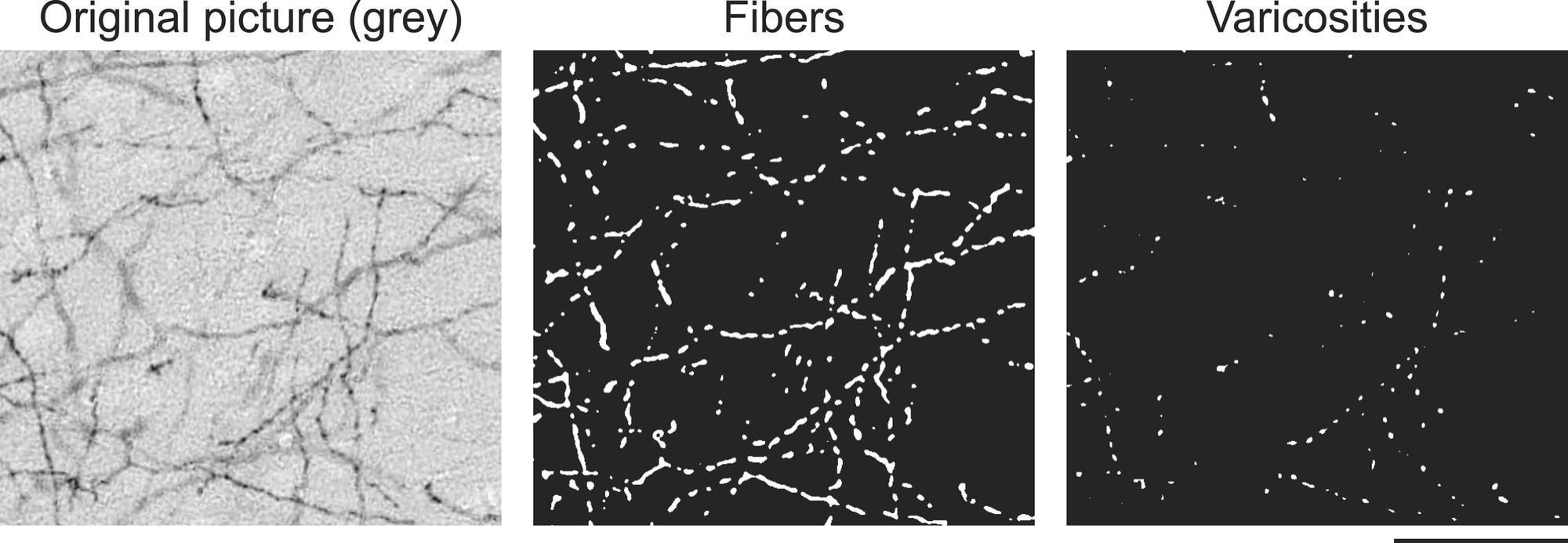
Original picture (grey)
Fibers
Varicosities

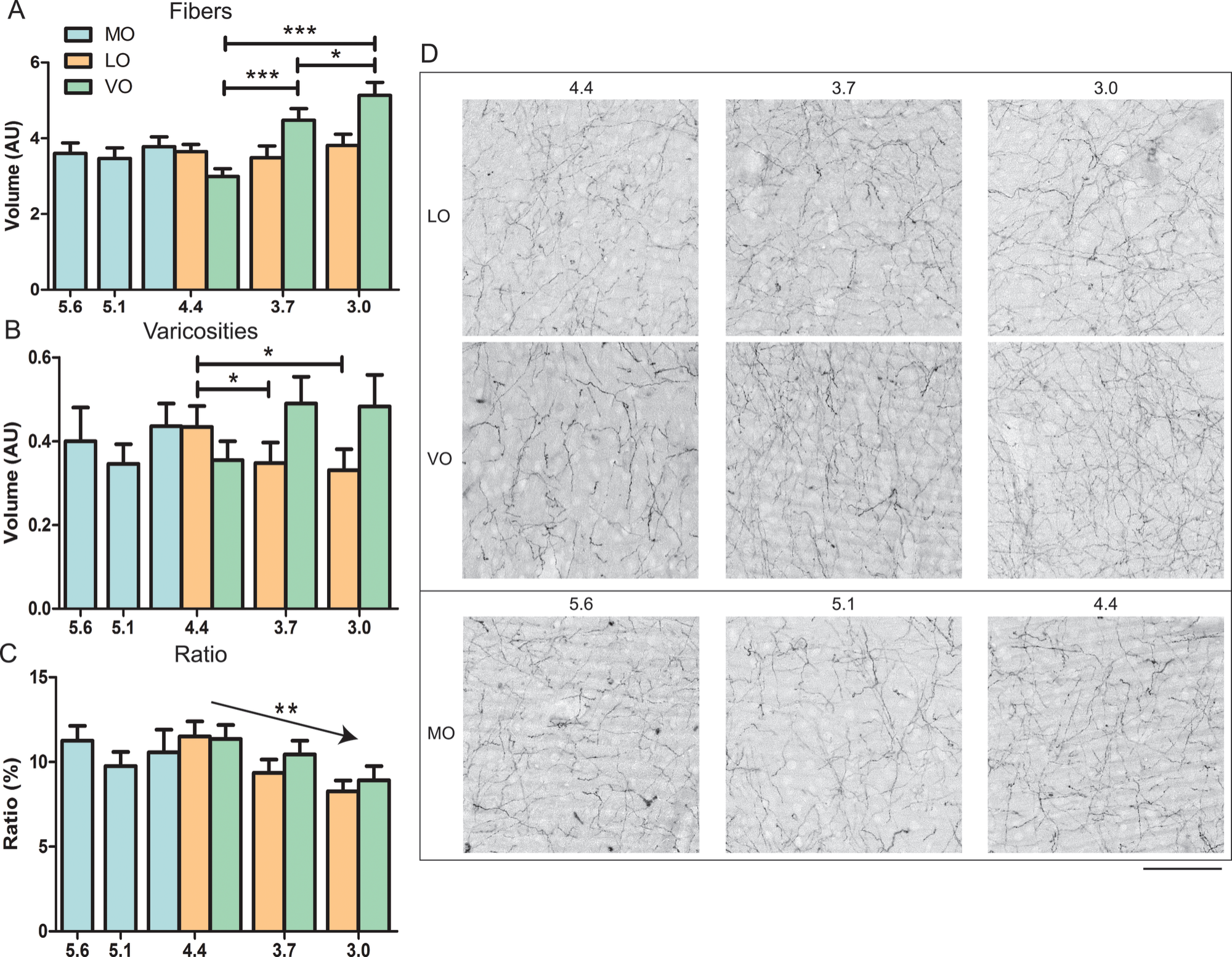
A
Fibers
MO
LO
VO
***
*
***
Volume (AU)
6
4
2
0
5.6
5.1
4.4
3.7
3.0
B
Varicosities
*
*
Volume (AU)
0.6
0.4
0.2
0.0
5.6
5.1
4.4
3.7
3.0
C
Ratio
**
Ratio (%)
15
10
5
0
5.6
5.1
4.4
3.7
3.0
D
4.4
3.7
3.0
LO
VO
5.6
5.1
4.4
MO

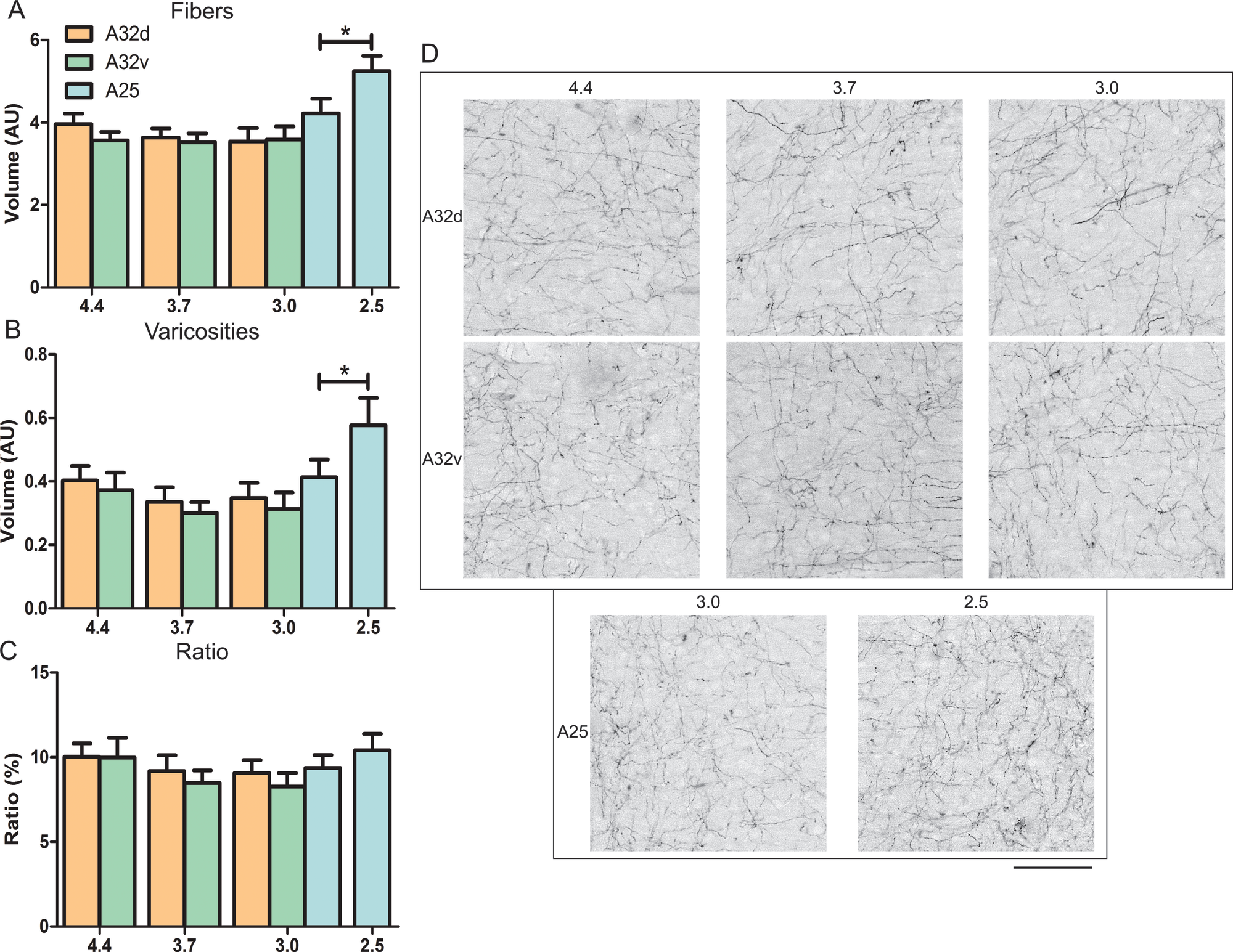
A
Fibers
A32d
A32v
A25
*
Volume (AU)
6
4
2
0
4.4
3.7
3.0
2.5
B
Varicosities
*
Volume (AU)
0.8
0.6
0.4
0.2
0.0
4.4
3.7
3.0
2.5
C
Ratio
Ratio (%)
15
10
5
0
4.4
3.7
3.0
2.5
D
4.4
3.7
3.0
A32d
A32v
3.0
2.5
A25

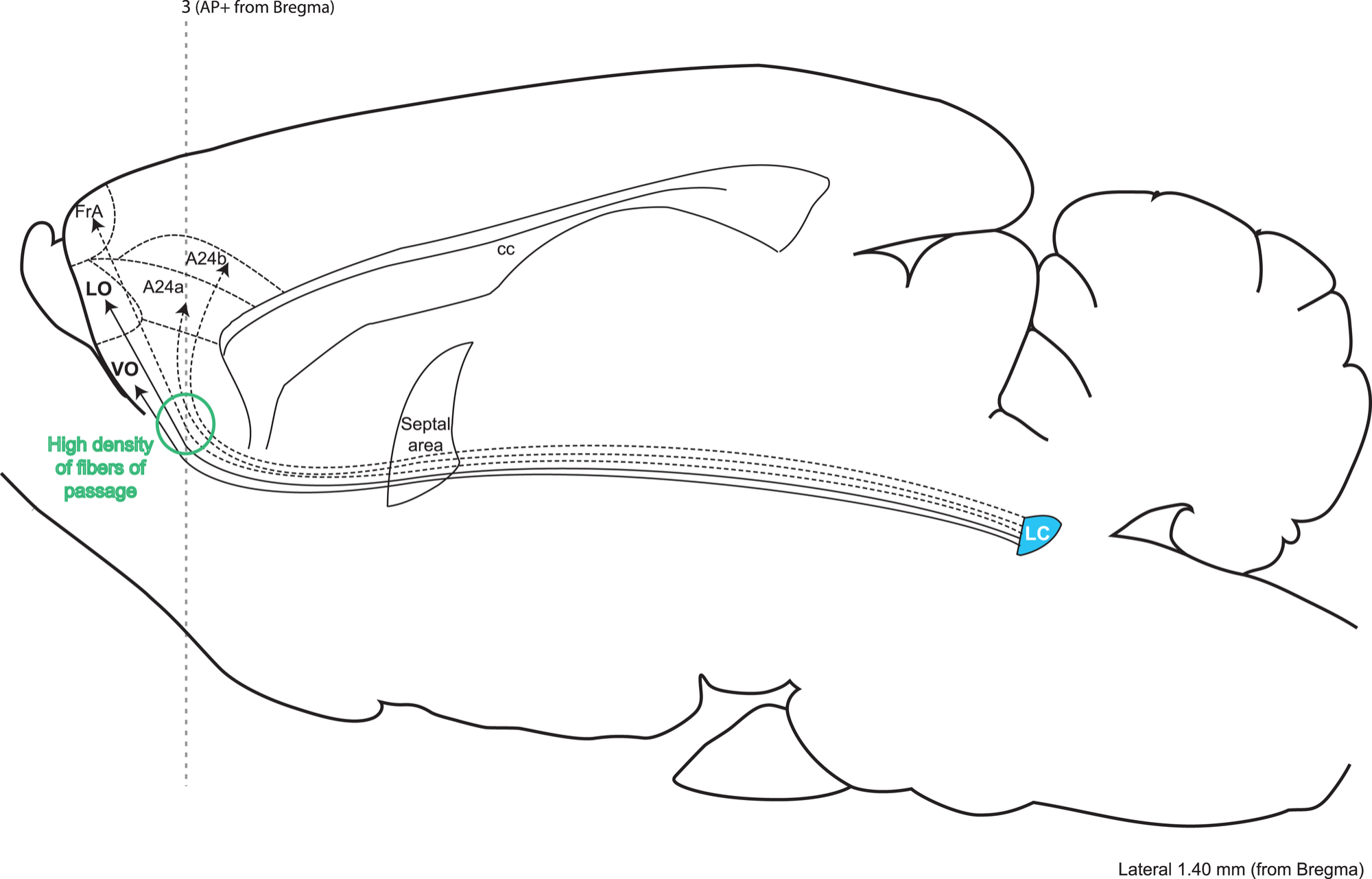
3 (AP+ from Bregma)
FrA
A24b
A24a
LO
VO
cc
Septal
area
High density
of fibers of
passage
LC
Lateral 1.40 mm (from Bregma)